

Magnetic susceptibilities in a family of $S = \frac{1}{2}$ kagome antiferromagnets

T. Ono,^{1,*} K. Morita,¹ M. Yano,¹ H. Tanaka,¹ K. Fujii,² H. Uekusa,² Y. Narumi,³ and K. Kindo⁴

¹*Department of Physics, Tokyo Institute of Technology, Meguro-ku, Tokyo 152-8551, Japan*

²*Department of Chemistry and Materials Science, Tokyo Institute of Technology, Meguro-ku, Tokyo 152-8551, Japan*

³*Institute for Material Research, Tohoku University, Aoba-ku, Sendai 980-8577, Japan*

⁴*Institute for Solid State Physics, The University of Tokyo, Kashiwa, Chiba 277-8581, Japan*

(Received 19 January 2009; published 6 May 2009)

Hexagonal antiferromagnets $\text{Cs}_2\text{Cu}_3\text{MF}_{12}$ ($M = \text{Zr, Hf, and Sn}$) have uniform kagome lattices of Cu^{2+} with $S = 1/2$, whereas $\text{Rb}_2\text{Cu}_3\text{SnF}_{12}$ has a $2a \times 2a$ enlarged cell as compared to the uniform kagome lattice. The crystal data of $\text{Cs}_2\text{Cu}_3\text{SnF}_{12}$ synthesized in the present work are reported. We performed magnetic-susceptibility measurements on this family of kagome antiferromagnet using single crystals. In the $\text{Cs}_2\text{Cu}_3\text{MF}_{12}$ systems, structural phase transitions were observed at $T_i = 225, 172,$ and 185 K for $M = \text{Zr, Hf, and Sn}$, respectively. The magnetic susceptibilities observed for $T > T_i$ are almost perfectly described using theoretical results obtained by exact diagonalization for the 24-site kagome cluster with $J/k_B = 244, 266,$ and 240 K, respectively. Magnetic ordering accompanied by the weak ferromagnetic moment occurs at $T_N = 23.5, 24.5,$ and 20.0 K, respectively. The origins of the weak ferromagnetic moment should be ascribed to the lattice distortion that breaks the hexagonal symmetry of the exchange network for $T < T_i$ and the Dzyaloshinsky-Moriya interaction. $\text{Rb}_2\text{Cu}_3\text{SnF}_{12}$ is magnetically described as a modified kagome antiferromagnet with four types of neighboring exchange interactions. Neither structural nor magnetic phase transition was observed in $\text{Rb}_2\text{Cu}_3\text{SnF}_{12}$. Its magnetic ground state was found to be a spin singlet with a triplet gap. Using exact diagonalization for a 12-site kagome cluster, we analyzed the magnetic susceptibility and evaluated individual exchange interactions. The causes leading to the different ground states in $\text{Cs}_2\text{Cu}_3\text{SnF}_{12}$ and $\text{Rb}_2\text{Cu}_3\text{SnF}_{12}$ are discussed.

DOI: [10.1103/PhysRevB.79.174407](https://doi.org/10.1103/PhysRevB.79.174407)

PACS number(s): 75.10.Jm, 75.40.Cx

I. INTRODUCTION

The Heisenberg kagome antiferromagnet (HKAF) has been attracting considerable attention from the viewpoints of frustration and quantum effects.^{1,2} In the classical spin model, three spins on a local triangle form a 120° structure as in the case of the Heisenberg triangular antiferromagnet (HTAF). However, different from the HTAF, the classical HKAF has infinite ground states in the case of the nearest-neighbor exchange interaction because of the flexibility of configuration of neighboring two 120° structures. When the next-nearest-neighbor (NNN) interaction is switched on, the so-called $q=0$ or $\sqrt{3} \times \sqrt{3}$ structure is stabilized in accordance with the sign of the NNN interaction.³ The HKAF with the nearest-neighbor interaction has been actively studied theoretically. It was predicted that for classical and large spins, thermal and quantum fluctuations stabilize the $\sqrt{3} \times \sqrt{3}$ structure without the help of the NNN interaction,^{4,5} whereas for small spin values as $S = 1/2$ or 1 , strong quantum fluctuation leads to the disordered ground state.⁶⁻¹³ Careful analysis and numerical calculation for the $S = 1/2$ case revealed that triplet excitations are gapped, but there exists the continuum of low-lying singlet states below the triplet gap.¹⁴⁻¹⁸ The magnitude of the triplet gap could be as small as $J/20$, if any, where the exchange constant J is defined as $\mathcal{H}_{\text{ex}} = \sum_{\langle i,j \rangle} J_{ij} \mathbf{S}_i \cdot \mathbf{S}_j$. Valence-bond crystal represented by a periodic arrangement of singlet dimers has been proposed as the ground state of $S = 1/2$ HKAF.¹⁹⁻²³ Another theory based on the resonating valence bond or the gapless critical spin liquid has also been proposed.²⁴⁻²⁸

For $S = 1/2$ HKAF, numerical calculation demonstrated that the magnetic susceptibility has a sharp rounded maxi-

mum at $T_{\text{max}} \approx (1/6)J/k_B$ and decreases toward zero with decreasing temperature.^{9,28,29} The temperature T_{max} giving the susceptibility maximum is considerably smaller than J/k_B owing to the strong frustration. These unusual features of the magnetic susceptibility have not been sufficiently verified.

The experimental studies on the HKAF have first been concentrated on jarosites with large spin values.³⁰⁻⁴² The chemical formula of the jarosites is expressed as $AM_3(\text{OH})_6(\text{SO}_4)_2$, where A is a monovalent ion such as K^+ and $M = \text{Fe}^{3+}$ ($S = 5/2$) or Cr^{3+} ($S = 3/2$). In many jarosites, the ordered state with the $q=0$ structure has been observed contrary to the theoretical prediction.^{32,35,37,42} The $q=0$ structure was also observed in hexagonal tungsten bronze (HTB)-type FeF_3 with the kagome layer.⁴³ The $q=0$ structure observed in the jarosites and HTB- FeF_3 can be ascribed to the antisymmetric interaction of the Dzyaloshinsky-Moriya (DM) type with alternating \mathbf{D} vectors.^{42,44} In iron jarosite with $A = \text{D}_3\text{O}^+$, spin freezing behavior was observed.^{45,46} (m -MPYNN) $\text{BF}_4 \cdot \frac{1}{3}(\text{acetone})$ is known as the composite $S = 1$ HKAF with the gapped singlet ground state.⁴⁷ In this organic system, two radical spins coupled through strong ferromagnetic interaction form the $S = 1$ state and the composite spins are placed on a modified kagome lattice.⁴⁸

In contrast to theoretical studies, the experimental studies on the $S = 1/2$ HKAF are limited. Experiments were performed on $\text{Cu}_3\text{V}_2\text{O}_7(\text{OH})_2 \cdot 2\text{H}_2\text{O}$,⁴⁹ $[\text{Cu}_3(\text{titmb})_2(\text{CH}_3\text{CO}_2)_6] \cdot \text{H}_2\text{O}$,⁵⁰ and $\beta\text{-Cu}_3\text{V}_2\text{O}_8$ (Ref. 51) that have a kagome or related lattice. Because the kagome net is distorted into an orthorhombic form in $\text{Cu}_3\text{V}_2\text{O}_7(\text{OH})_2 \cdot 2\text{H}_2\text{O}$ and buckled like a staircase in

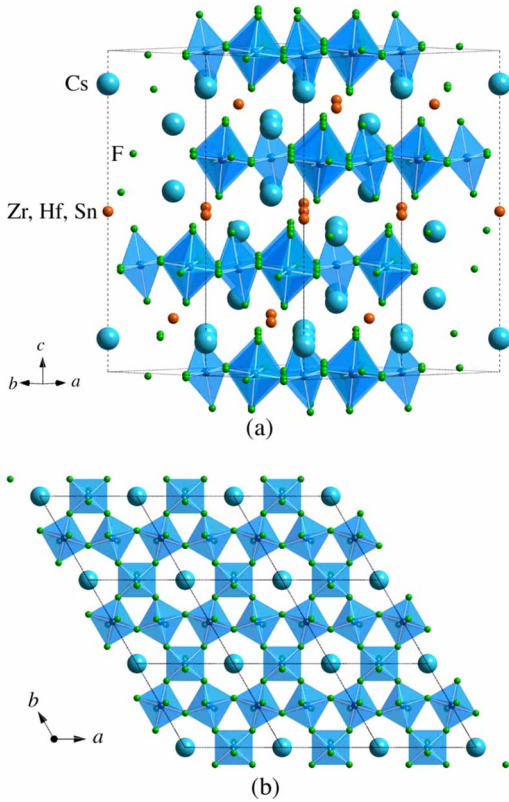


FIG. 1. (Color online) (a) Crystal structure of $\text{Cs}_2\text{Cu}_3\text{MF}_{12}$ ($M = \text{Zr}, \text{Hf}, \text{and Sn}$) viewed along the $[1, 1, 0]$ direction and (b) its projection onto the c plane. Shaded octahedra represent CuF_6 octahedra. Dotted lines denote the unit cell.

$\beta\text{-Cu}_3\text{V}_2\text{O}_8$, the exchange network is fairly anisotropic. For $[\text{Cu}_3(\text{titmb})_2(\text{CH}_3\text{CO}_2)_6] \cdot \text{H}_2\text{O}$, the nearest-neighbor exchange interaction is ferromagnetic.⁵² The above-mentioned exotic ground state has not been observed in these systems.

Shores *et al.*⁵³ reported the synthesis and magnetic properties of herbertsmithite $\text{ZnCu}_3(\text{OH})_6\text{Cl}_2$ that has the uniform kagome lattice. Since then, herbertsmithite has been attracting considerable attention.^{29,54–63} No magnetic ordering occurs down to 50 mK because of strong spin frustration.⁵⁴ However, the magnetic susceptibility exhibits a rapid increase at low temperatures, which was ascribed to idle spins produced by the intersite mixing of 5–10 % between Cu^{2+} and Zn^{2+} .^{29,55,56,58,59} NMR experiments on uniaxially aligned and ^{17}O -enriched powder samples revealed that the Knight shift proportional to the intrinsic magnetic susceptibility of the host lattice exhibits a broad maximum at 50–100 K and decreases with decreasing temperature.^{60,61} However, owing to the lattice disorder, the intrinsic magnetic susceptibility of herbertsmithite is still unclear.

The cupric compound $\text{Cs}_2\text{Cu}_3\text{MF}_{12}$ ($M = \text{Zr}$ and Hf) is a new family of $S = 1/2$ HKAF, which has a uniform kagome lattice at room temperature.^{64,65} Müller and Müller⁶⁴ synthesized $\text{Cs}_2\text{Cu}_3\text{ZrF}_{12}$ and $\text{Cs}_2\text{Cu}_3\text{HfF}_{12}$ and determined the crystal structures at room temperature. These compounds are crystallized in hexagonal structure (space group $R\bar{3}m$).⁶⁴ Figure 1 shows the crystal structure of the hexagonal $\text{Cs}_2\text{Cu}_3\text{MF}_{12}$ family and its projection onto the c plane. As

shown in Fig. 1(b), CuF_6 octahedra are linked in the c plane sharing corners. Magnetic Cu^{2+} ions with $S = 1/2$ located at the center of the octahedra form a uniform kagome layer in the c plane. The nearest-neighbor exchange interactions are equivalent because all the Cu^{2+} ions are crystallographically equivalent. CuF_6 octahedra are elongated along the principal axes, which makes an angle of approximately 11° with the c axis. Because the elongated axes of the octahedra are approximately parallel to the c axis, the hole orbitals $d(x^2 - y^2)$ of Cu^{2+} spread in the kagome layer. The nearest-neighbor superexchange interaction J through F^- ion in the kagome layer is antiferromagnetic and strong⁶⁵ because the bond angle of the superexchange $\text{Cu}^{2+} - \text{F}^- - \text{Cu}^{2+}$ is approximately 140° . The ferromagnetic superexchange occurs only when the bond angle is close to 90° . The interlayer exchange interaction J' should be much smaller than J because magnetic Cu^{2+} layers are sufficiently separated by nonmagnetic Cs^+ , M^{4+} , and F^- layers. Thus, the present hexagonal $\text{Cs}_2\text{Cu}_3\text{MF}_{12}$ family can be expected to be quasi-two-dimensional $S = 1/2$ HKAF. However, these systems undergo structural phase transitions at $T_i \approx 220$ and 170 K, respectively, and also magnetic phase transitions at $T_N \approx 24$ K.⁶⁵ In this study, we synthesized $\text{Cs}_2\text{Cu}_3\text{SnF}_{12}$ that has the same crystal structure as $\text{Cs}_2\text{Cu}_3\text{ZrF}_{12}$ and $\text{Cs}_2\text{Cu}_3\text{HfF}_{12}$ and performed precise magnetic-susceptibility measurements on $\text{Cs}_2\text{Cu}_3\text{MF}_{12}$, with $M = \text{Zr}, \text{Hf}, \text{and Sn}$, using high quality single crystals. In this paper, we will report the results. As shown below, the high-temperature susceptibilities of these systems can be almost perfectly described using the theoretical calculations on $S = 1/2$ HKAF.

In the previous letter, we reported the crystal structure and magnetic properties of $\text{Rb}_2\text{Cu}_3\text{SnF}_{12}$.⁶⁶ $\text{Rb}_2\text{Cu}_3\text{SnF}_{12}$ has the hexagonal structure (space group $R\bar{3}$) which is closely related to the structure of the above-mentioned $\text{Cs}_2\text{Cu}_3\text{MF}_{12}$. The unit cell in the kagome layer is enlarged to $2a \times 2a$. Consequently, the kagome lattice is modified to have four types of neighboring exchange interaction. Figure 2 shows a comparison of the crystal structures of $\text{Cs}_2\text{Cu}_3\text{SnF}_{12}$ and $\text{Rb}_2\text{Cu}_3\text{SnF}_{12}$. The structures are viewed along the c axis and fluorine ions located outside the kagome layer are omitted so that magnetic Cu^{2+} ions and exchange pathways are visible. From magnetic-susceptibility and high-field magnetization measurements, it was found that the magnetic ground state of $\text{Rb}_2\text{Cu}_3\text{SnF}_{12}$ is a spin singlet with the triplet gap. In this paper, we will show the details of the analysis of the magnetic susceptibilities by exact diagonalization for a 12-site kagome cluster.

The arrangement of this paper is as follows. In Sec. II, the experimental procedures and the crystal structure of newly synthesized $\text{Cs}_2\text{Cu}_3\text{SnF}_{12}$ are described. The results of the magnetic-susceptibility measurements performed on $\text{Cs}_2\text{Cu}_3\text{MF}_{12}$ and $\text{Rb}_2\text{Cu}_3\text{SnF}_{12}$ are presented in Sec. III. Analyses of the magnetic-susceptibility data and discussion are also given in Sec. III. Section IV is devoted to the conclusion.

II. EXPERIMENTAL DETAILS

$A_2\text{Cu}_3\text{MF}_{12}$ crystals, with $M = \text{Zr}, \text{Hf}, \text{and Sn}$ and $A = \text{Cs}$ and Rb , were synthesized in accordance with the chemical

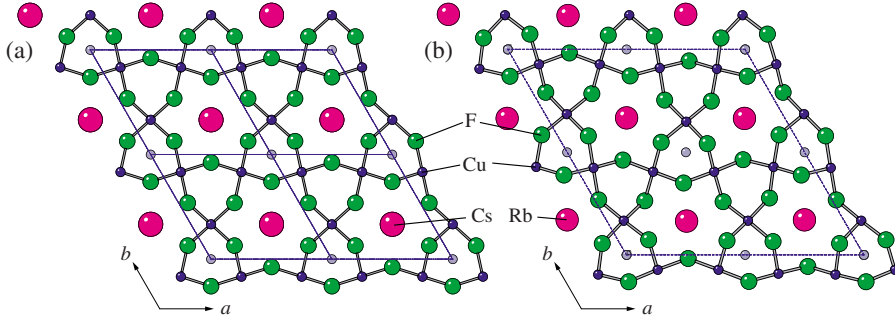


FIG. 2. (Color online) Crystal structures of (a) $\text{Cs}_2\text{Cu}_3\text{SnF}_{12}$ and (b) $\text{Rb}_2\text{Cu}_3\text{SnF}_{12}$ viewed along the c axis, where fluorine ions located outside the kagome layer are omitted. Dashed lines denote the unit cell.

reaction $2\text{AF} + 3\text{CuF}_2 + \text{MF}_4 \rightarrow \text{A}_2\text{Cu}_3\text{MF}_{12}$. AF , CuF_2 , and MF_4 were dehydrated by heating in vacuum at $\sim 100^\circ\text{C}$. The materials were packed into a Pt tube of 9.6 mm inner diameter and 70–100 mm length at the ratio of 3:3:2. One end of the Pt tube was welded and the other end was tightly folded with pliers. Single crystals were grown from the melt. For $\text{Cs}_2\text{Cu}_3\text{ZrF}_{12}$ and $\text{Cs}_2\text{Cu}_3\text{HfF}_{12}$, the temperature of the furnace was lowered from 750°C to 500°C for 4 d and from 800°C to 550°C for $\text{Cs}_2\text{Cu}_3\text{SnF}_{12}$ and $\text{Rb}_2\text{Cu}_3\text{SnF}_{12}$. Transparent light-green crystals are platelet shaped. For $\text{Rb}_2\text{Cu}_3\text{SnF}_{12}$, crystals with the size of $9 \times 9 \times 1 \text{ mm}^3$ were obtained.

The $\text{Cs}_2\text{Cu}_3\text{ZrF}_{12}$ and $\text{Cs}_2\text{Cu}_3\text{HfF}_{12}$ crystals obtained were identified by x-ray powder diffractions. The crystal data for $\text{Rb}_2\text{Cu}_3\text{SnF}_{12}$ have been reported in the previous paper.⁶⁶ The crystal structure of $\text{Cs}_2\text{Cu}_3\text{SnF}_{12}$ has not been reported to date. Therefore, we analyzed the structural of $\text{Cs}_2\text{Cu}_3\text{SnF}_{12}$ at room temperature using a RIGAKU R-AXIS RAPID three-circle diffractometer equipped with an imaging plate area detector. Monochromatic $\text{Mo K}\alpha$ radiation was used as an x-ray source. Data integration and global-cell refinements were performed using data in the range of $3.00^\circ < \theta < 27.47^\circ$, and multiscan empirical absorption correction was also performed. The total number of reflections observed was 2904. 290 reflections were found to be independent and 282 reflections were determined to satisfy the criterion $I > 2\sigma(I)$. Structural parameters were refined by the full-matrix least-squares method using SHELXL-97 software. The final R indices obtained were $R=0.0135$ and $wR=0.0325$. $\text{Cs}_2\text{Cu}_3\text{SnF}_{12}$ was found to be isostructural to $\text{Cs}_2\text{Cu}_3\text{ZrF}_{12}$ and $\text{Cs}_2\text{Cu}_3\text{HfF}_{12}$ (see Fig. 1). The lattice constants of $\text{Cs}_2\text{Cu}_3\text{SnF}_{12}$ are listed in Table I together with those of $\text{Cs}_2\text{Cu}_3\text{ZrF}_{12}$, $\text{Cs}_2\text{Cu}_3\text{HfF}_{12}$, and $\text{Rb}_2\text{Cu}_3\text{SnF}_{12}$. Fractional atomic coordinates and equivalent isotropic displacement parameters for $\text{Cs}_2\text{Cu}_3\text{SnF}_{12}$ are shown in Table II. Lattice constants a and c are both smaller than those for $\text{Cs}_2\text{Cu}_3\text{ZrF}_{12}$ and $\text{Cs}_2\text{Cu}_3\text{HfF}_{12}$, which have almost the same lattice constants.

TABLE I. Lattice constants a and c of $\text{Cs}_2\text{Cu}_3\text{MF}_{12}$ ($M=\text{Zr}$, Hf , and Sn) and $\text{Rb}_2\text{Cu}_3\text{ZrF}_{12}$ in \AA unit.

	$M=\text{Zr}$ ^a	$M=\text{Hf}$ ^a	$M=\text{Sn}$ ^b	$\text{Rb}_2\text{Cu}_3\text{SnF}_{12}$ ^c
a	7.166	7.163	7.142(4)	13.917(2)
c	20.46	20.49	20.381(14)	20.356(3)

^aReference 64.

^bPresent work.

^cReference 66.

The magnetic susceptibilities of the present four systems were measured in the temperature range of 1.8–400 K using a superconducting quantum interference device (SQUID) magnetometer (Quantum Design MPMS XL). High-field magnetization measurement on $\text{Rb}_2\text{Cu}_3\text{SnF}_{12}$ was performed by an induction method with a multilayer pulse magnet at the Institute for Solid State Physics, The University of Tokyo. Magnetic fields were applied parallel and perpendicular to the c axis in both experiments.

III. RESULTS AND DISCUSSIONS

A. $\text{Cs}_2\text{Cu}_3\text{MF}_{12}$ ($M=\text{Zr}$, Hf , and Sn)

$\text{Cs}_2\text{Cu}_3\text{MF}_{12}$ ($M=\text{Zr}$, Hf , and Sn) has the uniform kagome lattice at room temperature. Figure 3 shows the temperature dependences of magnetic susceptibilities χ in these three systems. External magnetic field of $H=1 \text{ T}$ was applied for $H\parallel c$ and $H\perp c$. Note that $1M \text{ Cs}_2\text{Cu}_3\text{MF}_{12}$ contains $3M \text{ Cu}^{2+}$ ions. The susceptibility data were corrected for the diamagnetism χ_{dia} of core electrons and the Van Vleck paramagnetism. The diamagnetic susceptibilities of individual ions were taken from the literature.⁶⁷ The Van Vleck paramagnetic susceptibility was calculated using $\chi_{\text{VV}}^{\mu} = -(N\mu_B^2/\lambda)\Delta g_{\mu} = 3.14 \times 10^{-4}\Delta g_{\mu} \text{ emu/Cu}^{2+} \text{ mol}$, where $\lambda = -829 \text{ cm}^{-1}$ is the coefficient of the spin-orbit coupling for Cu^{2+} and $\Delta g_{\mu} = g_{\mu} - 2$ is the anisotropy of the g factor. To obtain the g factors in the present systems, we performed electron-spin-resonance (ESR) measurements, but no spectrum was observed owing to the extremely large linewidth.⁶⁸ Therefore, the g factors and χ_{VV}^{μ} were determined self-consistently as $\chi_{\parallel c}/\chi_{\perp c} = (g_{\parallel c}/g_{\perp c})^2$ in the temperature range higher than the structural phase-transition temperature T_i . The g factors obtained are listed in Table III. These g factors are consistent with $g_{\parallel} = 2.48$ and $g_{\perp} = 2.09$ measured in K_2CuF_4 and Rb_2CuF_4 with the K_2NiF_4 structure,⁶⁹ where g_{\parallel}

TABLE II. Fractional atomic coordinates and equivalent isotropic displacement parameters (\AA^2) for $\text{Cs}_2\text{Cu}_3\text{SnF}_{12}$.

Atom	x	y	z	U_{eq}
Cs	0	0	0.1060(1)	0.032(1)
Cu	0.5	0	0	0.011(1)
Sn	0	0	0.5	0.013(1)
F(1)	0.2042(2)	-0.2042(2)	0.9845(1)	0.022(1)
F(2)	0.1312(2)	-0.1312(2)	0.4465(1)	0.036(1)

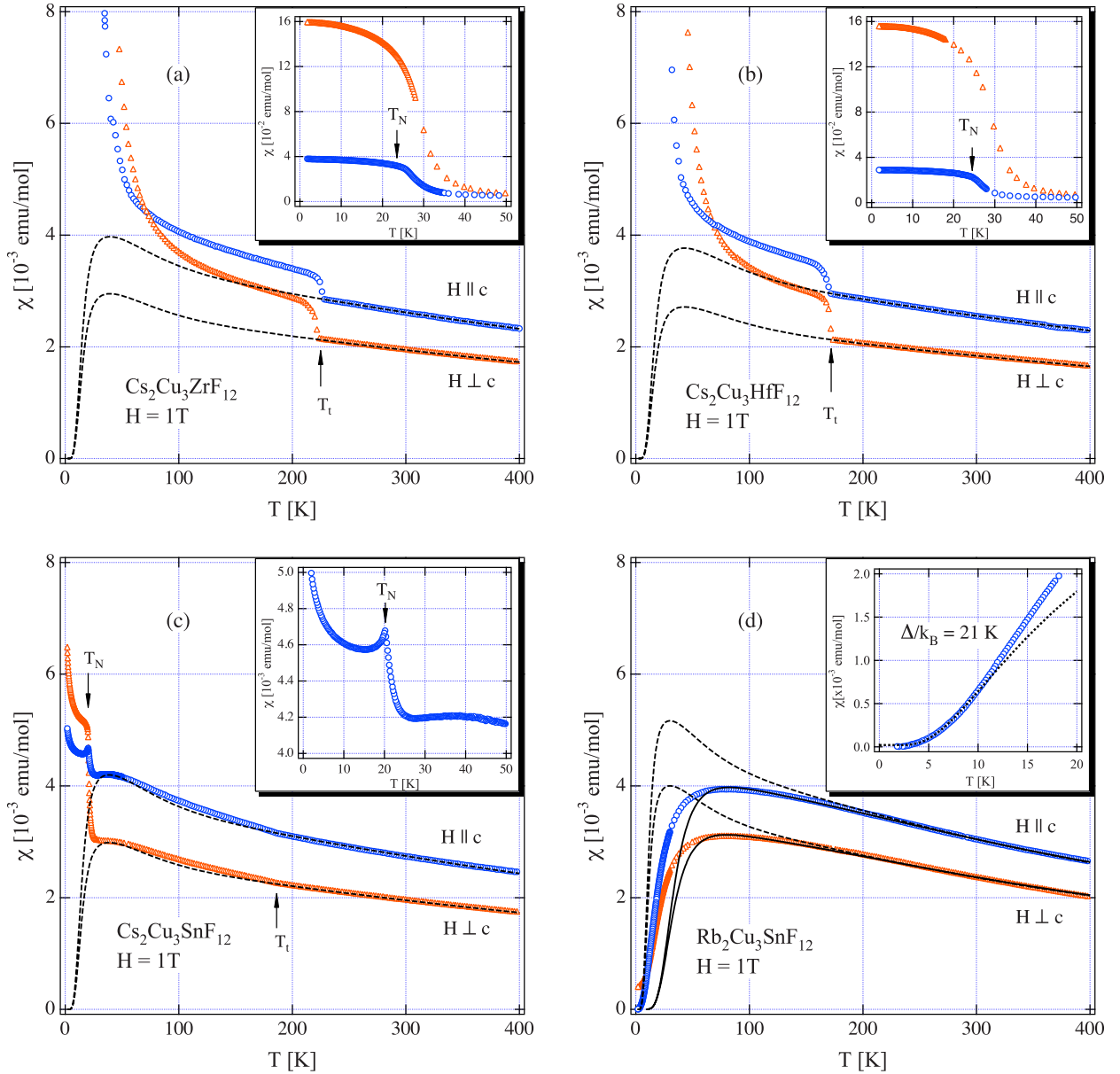


FIG. 3. (Color online) Temperature dependences of magnetic susceptibilities of (a) $\text{Cs}_2\text{Cu}_3\text{ZrF}_{12}$, (b) $\text{Cs}_2\text{Cu}_3\text{HfF}_{12}$, (c) $\text{Cs}_2\text{Cu}_3\text{SnF}_{12}$, and (d) $\text{Rb}_2\text{Cu}_3\text{SnF}_{12}$ measured at $H=1$ T for $H\parallel c$ and $H\perp c$. Arrows in (a)–(c) denote structural and magnetic phase-transition temperatures T_t and T_N . Dashed lines denote the fits using the theoretical susceptibilities for the uniform HKAF obtained from exact diagonalization for the 24-site kagome cluster (Ref. 29). The magnetic parameters used for the fits for Cs compounds are given in Table III and those for $\text{Rb}_2\text{Cu}_3\text{SnF}_{12}$ are shown in the text. Insets of (a) and (d) are low-temperature susceptibilities. Solid lines in (d) denote the results obtained by exact diagonalization for a 12-site kagome cluster with the exchange parameters $J_1/k_B=234$ K, $J_2/k_B=211$ K, $J_3/k_B=187$ K, and $J_4/k_B=108$ K and $g_{\parallel}=2.44$ and $g_{\perp}=2.15$. The dotted line in the inset of (d) denotes the fit using Eq. (3) with $\Delta/k_B=21$ K.

and g_{\perp} are the g factors for the magnetic field parallel and perpendicular to the elongated axis of the CuF_6 octahedron, respectively.

With decreasing temperature from 400 K, the magnetic susceptibilities exhibit sudden jumps at $T_t=225$ and 172 K for $\text{Cs}_2\text{Cu}_3\text{ZrF}_{12}$ and $\text{Cs}_2\text{Cu}_3\text{HfF}_{12}$, respectively, while for $\text{Cs}_2\text{Cu}_3\text{SnF}_{12}$, the magnetic susceptibility displays a small bend anomaly at $T_t=185$ K. The phase transition at T_t is attributed to structural phase transition. Because small hysteresis was observed at T_t for $\text{Cs}_2\text{Cu}_3\text{ZrF}_{12}$ and $\text{Cs}_2\text{Cu}_3\text{HfF}_{12}$, the structural phase transition is of first order. For

$\text{Cs}_2\text{Cu}_3\text{SnF}_{12}$, the structural phase transition may be of second order because the susceptibility anomaly at T_t is continuous. We performed the structural analyses below T_t on $\text{Cs}_2\text{Cu}_3\text{ZrF}_{12}$ and $\text{Cs}_2\text{Cu}_3\text{SnF}_{12}$ by x-ray diffraction, but we did not succeed in obtaining definite results. For $\text{Cs}_2\text{Cu}_3\text{SnF}_{12}$, it is certain that the unit cell in the kagome layer is enlarged to $2a \times 2a$, as observed in $\text{Rb}_2\text{Cu}_3\text{SnF}_{12}$. However, it is unclear whether both structures are the same. For $\text{Cs}_2\text{Cu}_3\text{SnF}_{12}$, the value of $\eta=(\chi_{\parallel c}g_{\perp c}^2)/(\chi_{\perp c}g_{\parallel c}^2)$ does not change at T_t and remains unity down to 40 K, where the $g_{\parallel c}$ and $g_{\perp c}$ are the g factors for $T>T_t$. This indicates that the

angle between the elongated axis of CuF_6 octahedron and the c axis is almost unchanged at T_t . On the other hand, for $\text{Cs}_2\text{Cu}_3\text{ZrF}_{12}$ and $\text{Cs}_2\text{Cu}_3\text{HfF}_{12}$, the η value decreases just below T_t to $\eta=0.88$ and 0.87 , respectively. This implies that the angle between the elongated axis of CuF_6 octahedron and the c axis increases below T_t on average, i.e., $11^\circ \rightarrow 28^\circ$ and 27° for $\text{Cs}_2\text{Cu}_3\text{ZrF}_{12}$ and $\text{Cs}_2\text{Cu}_3\text{HfF}_{12}$, respectively.

With further decreasing temperature, the magnetic susceptibilities of $\text{Cs}_2\text{Cu}_3\text{ZrF}_{12}$ and $\text{Cs}_2\text{Cu}_3\text{HfF}_{12}$ increase below 50 K, which is indicative of magnetic ordering accompanied by small ferromagnetic moments. The magnetic phase-transition temperatures for both systems are approximately the same and are $T_N=23.5$ and 24.5 K, respectively. Because the anomaly of the magnetic susceptibility at T_N is not sharp in $\text{Cs}_2\text{Cu}_3\text{ZrF}_{12}$ and $\text{Cs}_2\text{Cu}_3\text{HfF}_{12}$, these Néel temperatures were determined by specific-heat measurements.⁶⁵ For $\text{Cs}_2\text{Cu}_3\text{SnF}_{12}$, the magnetic susceptibility has a rounded maximum at $T_{\max} \approx 38$ K as shown in the inset of Fig. 3(c) and exhibits a sharp cusp and a sharp increase at $T_N = 20.2$ K for $H \parallel c$ and $H \perp c$, respectively, indicative of three-dimensional (3D) magnetic ordering.

We compare our experimental results for $T_t < T < 400$ K to the theoretical susceptibility for the $S=1/2$ uniform HKAF obtained by Misguich and Sindzingre²⁹ from exact diagonalization for the 24-site kagome cluster. The dashed lines in Figs. 3(a)–3(c) denote the fits using the theoretical susceptibilities with the exchange parameters and the g factors given in Table III. Errors of the exchange parameters and the g factors are ± 2 K and ± 0.01 , respectively. The theoretical results provide an almost perfect description of the magnetic susceptibilities obtained for $T > T_t$. The magnetic susceptibility obeys approximately the Curie-Weiss law for $T_t < T < 400$ K. The magnitude of the effective Weiss constant Θ_{eff} obtained from the χ^{-1} vs T plot is 2.1–2.3 times as large as J/k_B , as predicted by theory for $T < 2J/k_B$.^{57,58} It was also observed that $k_B|\Theta_{\text{eff}}|/J$ increases a little with decreasing T_t , the lower limit of temperature range. For $\text{Cs}_2\text{Cu}_3\text{SnF}_{12}$, the agreement between theoretical and experimental susceptibilities is fairly good even below T_t . As shown in the inset of Fig. 3(c), the magnetic susceptibility exhibits a rounded maximum at $T_{\max} \approx 38$ K, which coincides with the theoretical result $T_{\max} \approx (1/6)J/k_B = 40$ K.^{9,29} This small T_{\max} as compared to J/k_B is characteristic of highly frustrated $S=1/2$ HKAF. Because the anomaly of the susceptibility at T_t is small in $\text{Cs}_2\text{Cu}_3\text{SnF}_{12}$, the change in the exchange interaction at T_t should be small. Below 30 K, the experimental susceptibility deviates significantly from the theoretical susceptibility owing to the occurrence of 3D ordering at $T_N=20.2$ K. The ratio of J/k_B to T_N is approximately 10 in the present three systems. This large $J/(k_B T_N)$

indicates the good two dimensionality and the presence of the strong frustration.

Magnetization curves exhibit hysteresis below T_N in the present three systems, which indicates that weak ferromagnetic moments appear below T_N . The weak ferromagnetic moment M_{wf} per Cu^{2+} for $H \parallel c$ is much smaller than that for $H \perp c$. The values of M_{wf} in $\text{Cs}_2\text{Cu}_3\text{ZrF}_{12}$ and $\text{Cs}_2\text{Cu}_3\text{HfF}_{12}$ are almost the same and $M_{\text{wf}} \approx 0.07\mu_B$ and $0.01\mu_B$ for $H \perp c$ and $H \parallel c$, respectively. The rapid increase in the magnetic susceptibility below 50 K in these two systems arises from the weak ferromagnetic moment. In $\text{Cs}_2\text{Cu}_3\text{SnF}_{12}$, $M_{\text{wf}} \approx 0.015\mu_B$ for $H \perp c$ and $M_{\text{wf}} \approx 0$ for $H \parallel c$. The weak ferromagnetic moment in $\text{Cs}_2\text{Cu}_3\text{SnF}_{12}$ is much smaller than those in $\text{Cs}_2\text{Cu}_3\text{ZrF}_{12}$ and $\text{Cs}_2\text{Cu}_3\text{HfF}_{12}$. Because the temperature variations of the magnetic susceptibilities of $\text{Cs}_2\text{Cu}_3\text{ZrF}_{12}$ and $\text{Cs}_2\text{Cu}_3\text{HfF}_{12}$ are similar to each other, the origin of the weak moment should be the same in these two systems, whereas the weak moment in $\text{Cs}_2\text{Cu}_3\text{SnF}_{12}$ is attributable to a different origin.

We consider two origins that give rise to the weak ferromagnetic moment. The first one is the DM interaction of the form $\mathcal{H}_{\text{DM}} = \sum_{\langle i,j \rangle} \mathbf{D}_{ij} \cdot [\mathbf{S}_i \times \mathbf{S}_j]$. Because the details of the crystal structure below T_t are unclear, we first consider the configuration of the \mathbf{D} vector in the high symmetric structure above T_t . There is no inversion center at the middle point of two neighboring magnetic ions in the kagome lattice. This situation differs from that in the triangular lattice. Thus, in general, the DM interaction is allowed in the kagome lattice. There exists a mirror plane that passes the middle points of neighboring two Cu^{2+} ions and is perpendicular to the line connecting these two ions. Therefore, the \mathbf{D} vector should be parallel to the mirror plane.⁷⁰ Because there are twofold screw axes along the $[1, 0, 0]$, $[0, 1, 0]$, and $[1, 1, 0]$ directions, the \mathbf{D} vectors change their directions alternately along these directions. Thus, the configuration of the \mathbf{D} vector should be as shown in Fig. 4. Two symbols \odot and \otimes in Fig. 4(a) and arrows in Fig. 4(b) denote the local positive directions of parallel and perpendicular components D^{\parallel} and D^{\perp} , respectively. There is no *a priori* relation between D^{\parallel} and D^{\perp} . The configuration of the \mathbf{D} vector shown in Fig. 4 is just the same as that discussed by Elhajal *et al.*⁴⁴ The parallel component D^{\parallel} acts as the easy-plane anisotropy that confines spins in the kagome layer and stabilizes the $q=0$ spin structure. The large arrows in Fig. 4(a) represent the $q=0$ spin structure that is stable for $D^{\parallel} > 0$. Because the c plane components of spins form the 120° structure, the parallel component D^{\parallel} does not give rise to the weak moment parallel to the kagome layer.

The perpendicular component D^{\perp} leads to the canting of spins from the kagome layer.⁴⁴ The canting angle φ is given by

TABLE III. Structural and magnetic phase-transition temperatures T_t (K) and T_N (K), and g factors and exchange constant J/k_B (K) for $T > T_t$ in $\text{Cs}_2\text{Cu}_3\text{MF}_{12}$ ($M = \text{Zr}, \text{Hf}, \text{and Sn}$).

	T_t	T_N	$g_{\parallel c}$	$g_{\perp c}$	J/k_B
$\text{Cs}_2\text{Cu}_3\text{ZrF}_{12}$	225	23.5	2.43	2.10	244
$\text{Cs}_2\text{Cu}_3\text{HfF}_{12}$	172	24.5	2.47	2.10	266
$\text{Cs}_2\text{Cu}_3\text{SnF}_{12}$	185	20.2	2.48	2.10	240

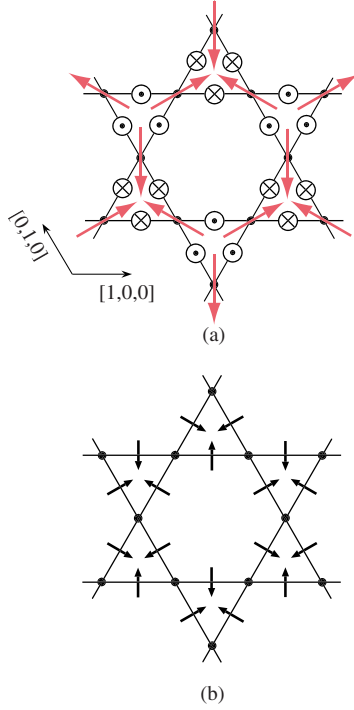


FIG. 4. (Color online) Arrangement of the \mathbf{D} vectors for $T > T_i$ in $\text{Cs}_2\text{Cu}_3\text{MF}_{12}$ systems. (a) The c axis component D^{\parallel} and (b) the c plane component D^{\perp} . Symbols \odot and \otimes in (a) and arrows in (b) denote the local positive directions of parallel and perpendicular components D^{\parallel} and D^{\perp} , respectively. Large arrows in (a) denote the $q=0$ spin structure stabilized when $D^{\parallel} > 0$.

$$\tan 2\varphi = \frac{2D^{\perp}}{\sqrt{3}J + D^{\parallel}}. \quad (1)$$

This spin canting produces the weak ferromagnetic moment of $M_{\text{wf}} = g\mu_B \langle S \rangle \sin \varphi$ perpendicular to the kagome layer. If the weak moments of neighboring layers do not cancel out, then weak net moment emerges along the c axis. Although the details of the crystal structure below T_i are unclear at present, it is considered that the configuration of the \mathbf{D} vector in the low-temperature crystal structure is close to that in the high-temperature crystal structure. Therefore, the weak ferromagnetic moment parallel to the c axis observed in the ordered states of $\text{Cs}_2\text{Cu}_3\text{ZrF}_{12}$ and $\text{Cs}_2\text{Cu}_3\text{HfF}_{12}$ can be attributed to the perpendicular component of the \mathbf{D} vector (D^{\perp}) for the DM interaction. Using Eq. (1) with $M_{\text{wf}} = 0.018$ and $0.012\mu_B/\text{Cu}^{2+}$ for $H \rightarrow 0$ observed in $\text{Cs}_2\text{Cu}_3\text{ZrF}_{12}$ and $\text{Cs}_2\text{Cu}_3\text{HfF}_{12}$, respectively, we obtain $D^{\perp}/J \approx 0.025$ and 0.017 , respectively. In $\text{Cs}_2\text{Cu}_3\text{SnF}_{12}$, no weak moment was observed for $H \parallel c$. This should be because the weak moments of neighboring layers cancel out. Sharp cusp anomaly at T_N as shown in the inset of Fig. 3(c) is often observed in jarosites^{33–35,42} and in the system where the weak moments cancel out.⁷¹

As the origin of the weak moment parallel to the kagome layer, we consider the orthorhombic distortion of the kagome lattice as discussed by Wang *et al.*⁷² and Yavors'kii *et al.*⁷³ This lattice distortion leads to two types of exchange interaction J_1 and J_2 as shown in Fig. 5. If the 3D ordering oc-

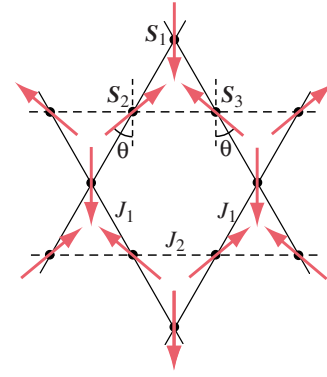


FIG. 5. (Color online) Anisotropic exchange network composed of J_1 (solid lines) and J_2 (dashed lines), which results from orthorhombic distortion of the kagome lattice. Large arrows represent the $q=0$ spin structure composed of three sublattice spins S_1 , S_2 , and S_3 . θ denotes the angle between the c plane component of $-S_1$ and that of S_2 or S_3 .

urs, the 120° structure is modified to be isosceles. The angle θ between the c plane component of $-S_1$ and that of S_2 or S_3 is given by

$$\cos \theta = \frac{J_1}{2J_2}. \quad (2)$$

Here, we assume that the c plane component of spins forms the triangular structure owing to the parallel component of the \mathbf{D} vector (D^{\parallel}) for the DM interaction. When the $q=0$ spin structure is realized, the weak moment of $M_{\text{wf}} = g\mu_B \langle S \rangle |2 \cos \theta - 1|/3$ is produced parallel to the kagome layer. Note that in the triangular lattice, the orthorhombic distortion of the lattice leads to the incommensurate helical spin structure,⁷⁴ which is not accompanied by the weak moment. The weak moment of $M_{\text{wf}} \approx 0.07\mu_B$ observed for $H \perp c$ in $\text{Cs}_2\text{Cu}_3\text{ZrF}_{12}$ and $\text{Cs}_2\text{Cu}_3\text{HfF}_{12}$ occurs when $J_1/J_2 \approx 1.2$ or 0.8 with $\langle S \rangle = 1/2$. Although the details of the low-temperature crystal structures of $\text{Cs}_2\text{Cu}_3\text{ZrF}_{12}$ and $\text{Cs}_2\text{Cu}_3\text{HfF}_{12}$ are unclear at present, it is probable that the hexagonal symmetry of the lattice is broken below T_i owing to the orthorhombic distortion, which leads to the anisotropic kagome lattice, as shown in Fig. 5. We infer that the weak moment parallel to the kagome layer arises from such spatially anisotropic exchange network. To describe the weak moments parallel and perpendicular to the kagome layer, we need both the DM interaction and the spatially anisotropic exchange network.

In $\text{Cs}_2\text{Cu}_3\text{SnF}_{12}$, the unit cell in the kagome layer is enlarged to $2a \times 2a$ below T_i , but the lattice still has the hexagonal symmetry. Consequently, the exchange network is modified to be that for $\text{Rb}_2\text{Cu}_3\text{SnF}_{12}$ shown in Fig. 6. In such exchange network that has the hexagonal symmetry, the weak moment does not appear. At present, we do not have clear explanation of the origin of the weak moment observed in $\text{Cs}_2\text{Cu}_3\text{SnF}_{12}$. It is possible that $\text{Cs}_2\text{Cu}_3\text{SnF}_{12}$ shows a domain structure below T_i and that the weak moment is induced in the domain boundaries where the hexagonal symmetry is locally broken.

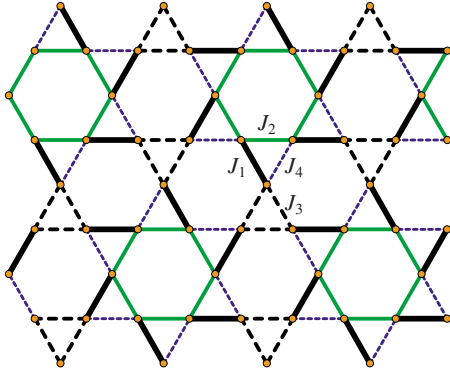


FIG. 6. (Color online) Exchange network in the kagome layer of $\text{Rb}_2\text{Cu}_3\text{SnF}_{12}$. Pinwheels composed of J_1 , J_2 , and J_4 interactions are connected by triangles of J_3 interactions.

B. $\text{Rb}_2\text{Cu}_3\text{SnF}_{12}$

As mentioned above, the chemical unit cell of $\text{Rb}_2\text{Cu}_3\text{SnF}_{12}$ is enlarged to $2a \times 2a$ in the kagome layer. In Fig. 2, we show a comparison of the crystal structures of $\text{Cs}_2\text{Cu}_3\text{SnF}_{12}$ and $\text{Rb}_2\text{Cu}_3\text{SnF}_{12}$. Figure 6 shows the exchange network in $\text{Rb}_2\text{Cu}_3\text{SnF}_{12}$. There are four types of nearest-neighbor exchange interactions. Because the bond angle α of the exchange pathway $\text{Cu}^{2+}-\text{F}^--\text{Cu}^{2+}$ ranges from $\alpha=123.9^\circ$ to 138.4° , the exchange interactions should be of the same order as those of $\text{Cs}_2\text{Cu}_3\text{MF}_{12}$. The exchange interactions $J_1 \sim J_4$ are labeled in decreasing order of α , i.e., in decreasing order of magnitude.

Figure 3(d) shows the temperature dependence of the magnetic susceptibilities of $\text{Rb}_2\text{Cu}_3\text{SnF}_{12}$ after the correction for the Curie-Weiss term owing to a small amount of impurities ($\approx 0.3\%$) and for the diamagnetism of core electrons and the Van Vleck paramagnetism. Raw susceptibility data of $\text{Rb}_2\text{Cu}_3\text{SnF}_{12}$ are shown in the previous paper.⁶⁶ With decreasing temperature, the magnetic susceptibilities of $\text{Rb}_2\text{Cu}_3\text{SnF}_{12}$ exhibit rounded maxima at $T_{\text{max}} \sim 70$ K and decrease rapidly. No magnetic ordering is observed. This result indicates clearly that the ground state is a singlet state with a triplet gap. The susceptibility for $H \parallel c$ is almost zero for $T \rightarrow 0$, whereas that for $H \perp c$ is finite.

In the present kagome family, elongated axes of CuF_6 octahedra incline alternately in the kagome layer as shown in Fig. 1(b). This leads to the staggered inclination of the principal axes of the \mathbf{g} tensor. When an external field is applied, the staggered component of the \mathbf{g} tensor produces the staggered field perpendicular to the external field.⁷⁵ The Zeeman interaction due to the staggered field and the DM interaction can have finite matrix elements between the singlet ground state and the excited triplet state because they are antisymmetric with respect to the interchange of the interacting spins. Thus, we infer that the ground state has a small amount of triplet component through these antisymmetric interactions when subjected to the external field parallel to the kagome layer. This gives rise to the finite susceptibility at $T=0$ for $H \perp c$.

As shown in Fig. 3(d), the magnetic susceptibility for $T > 150$ K agrees with the theoretical susceptibilities (dashed lines) for the $S=1/2$ uniform HKAF obtained by exact di-

agonalization for the 24-site kagome cluster with $J/k_B = 187$ K and $g_{\parallel}=2.43$ and $g_{\perp}=2.13$.²⁹ However, for $T < 150$ K, the agreement between experimental and theoretical susceptibilities is poor. The theoretical susceptibility exhibits a sharp rounded maximum at $T_{\text{max}} \approx (1/6)J/k_B \approx 30$ K, whereas the experimental susceptibility exhibits a broad maximum at $T_{\text{max}} \sim 70$ K. This is because exchange interactions in the kagome layer are not uniform.

Figure 6 shows the exchange network in the kagome layer of $\text{Rb}_2\text{Cu}_3\text{SnF}_{12}$. The network consists of pinwheels composed of J_1 , J_2 , and J_4 interactions, which are connected by triangles of J_3 interactions. One chemical unit cell in the kagome layer contains 12 spins. Then, we performed the exact diagonalization for the 12-site kagome cluster under the periodic boundary condition. First, we calculated the uniform case, $J_1=J_2=J_3=J_4=1$, to confirm the validity of our calculation. The result obtained is the same as that obtained by Elstner and Young⁹ from the exact diagonalization for the 12-site kagome cluster and close to the result for the 24-site kagome cluster obtained by Misguich and Sindzingre.²⁹ The comparison between susceptibilities obtained from the exact diagonalization for the 24- and 12-site kagome clusters is shown in Fig. 7(a). Both susceptibilities coincide for $k_B T/J_{\text{av}} > 0.5$ and a small difference between them is observed for $k_B T/J_{\text{av}} < 0.5$.

Figure 7(a) shows the susceptibilities calculated for $J_4/J_1=0.5, 0.75, 1$, and 1.5 , where we set $J_1=J_2=J_3$. In Fig. 7, temperature and susceptibilities are scaled using the average of exchange interactions $J_{\text{av}}=(1/4)\sum_i J_i$. Whether for $J_4/J_1 > 1$ or $J_4/J_1 < 1$, the maximum susceptibility χ_{max} decreases and T_{max} shifts toward the high-temperature side. The susceptibilities calculated for $J_4/J_1=0.5$ and 1.5 are close to the susceptibility observed in $\text{Rb}_2\text{Cu}_3\text{SnF}_{12}$. We also investigated the effects of J_2 and J_3 , setting the others equal. Figure 7(b) shows the susceptibilities calculated for $J_2/J_1=0.5, 1, 1.5$, and 2 . For $J_2/J_1 < 1$, χ_{max} increases and T_{max} decreases with decreasing J_2 , so that the rounded peak sharpens increasingly. The spin state for $J_2/J_1 \rightarrow 0$ is of interest. When $J_2/J_1 > 1$, the susceptibility increases like obeying the Curie law for $T \rightarrow 0$. In this case, six spins coupled through J_2 on a hexagon form a singlet state and three spins coupled through J_3 on a triangle form an $S=1/2$ state. This doublet state gives rise to the Curie law at low temperatures. Figure 7(c) shows the susceptibilities calculated for $J_3/J_1=0.5, 1, 1.5$, and 2 with $J_1=J_2=J_4$. The susceptibility is not largely influenced by J_3 .

When the hole orbitals $d(x^2-y^2)$ of neighboring Cu^{2+} ions are linked through the p orbital of F^- ion as in the present systems, the antiferromagnetic exchange interaction becomes stronger with increasing bonding angle α of the exchange pathway $\text{Cu}^{2+}-\text{F}^--\text{Cu}^{2+}$. It should be noted that the magnitude of the exchange constant for $\alpha=180^\circ$ was obtained to be $J/k_B \approx 390$ K in KCuF_3 (Ref. 76) and $\text{K}_3\text{Cu}_2\text{F}_7$.⁷⁷ The bonding angle α_i for the exchange interaction J_i in $\text{Rb}_2\text{Cu}_3\text{SnF}_{12}$ is as follows: $\alpha_1=138.4^\circ$, $\alpha_2=136.4^\circ$, $\alpha_3=133.4^\circ$, and $\alpha_4=123.9^\circ$. Hence, the condition $J_1 > J_2 > J_3 > J_4$ must be realized. Varying exchange parameters under this condition, we calculated susceptibility. The best fit for $T > T_{\text{max}} \sim 70$ K is obtained using $J_1/k_B=234(5)$ K, $J_2/k_B=211(5)$ K, $J_3/k_B=187(5)$ K, and $J_4/k_B=108(5)$ K, with $g_{\parallel}=2.44(1)$ and g_{\perp}

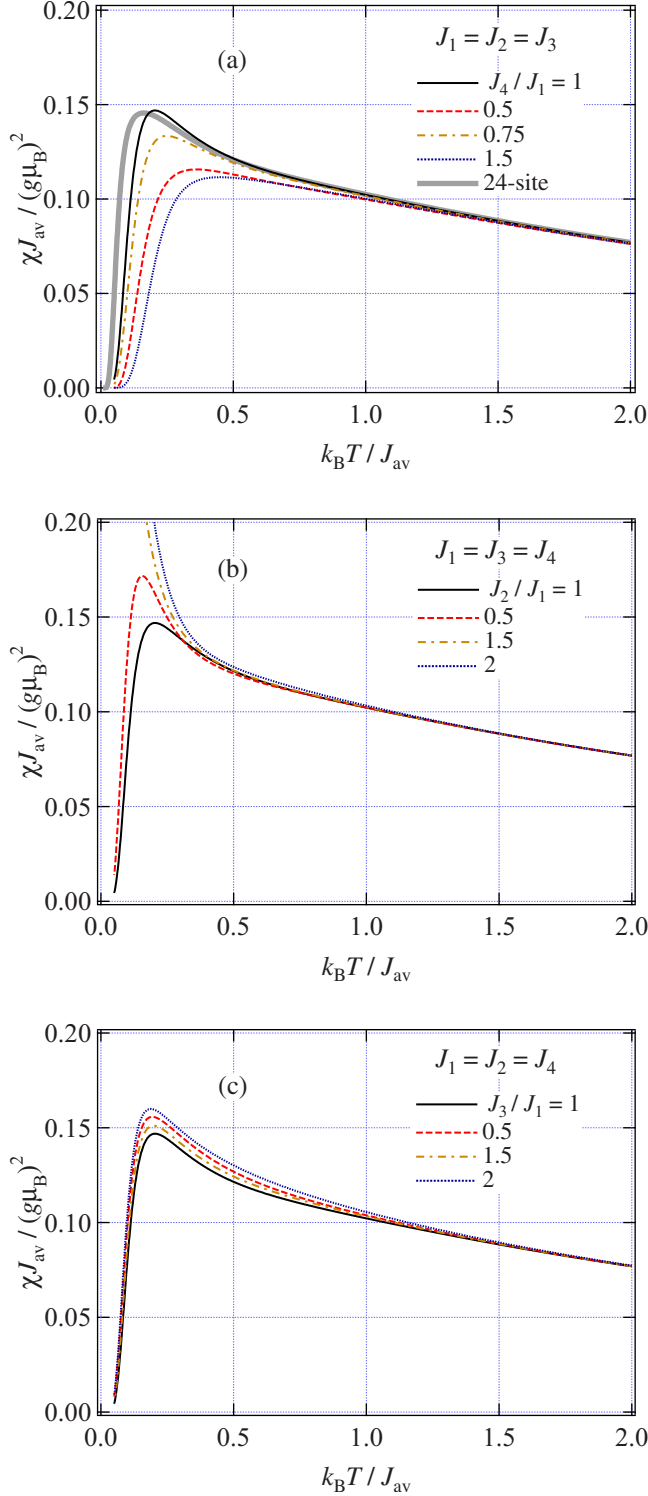


FIG. 7. (Color online) Temperature dependence of magnetic susceptibilities per site obtained by exact diagonalizations for 12-site kagome cluster (a) for $J_4/J_1=0.5, 0.75, 1$, and 1.5 with $J_1=J_2=J_3$, (b) for $J_2/J_1=0.5, 1, 1.5$, and 2 with $J_1=J_3=J_4$, and (c) for $J_3/J_1=0.5, 1, 1.5$, and 2 with $J_1=J_2=J_4$. Temperature is scaled using the average of the exchange interactions J_{av} . The thick solid line in (a) denotes the susceptibilities for the uniform HKAF obtained by exact diagonalization for the 24-site kagome cluster (Ref. 29).

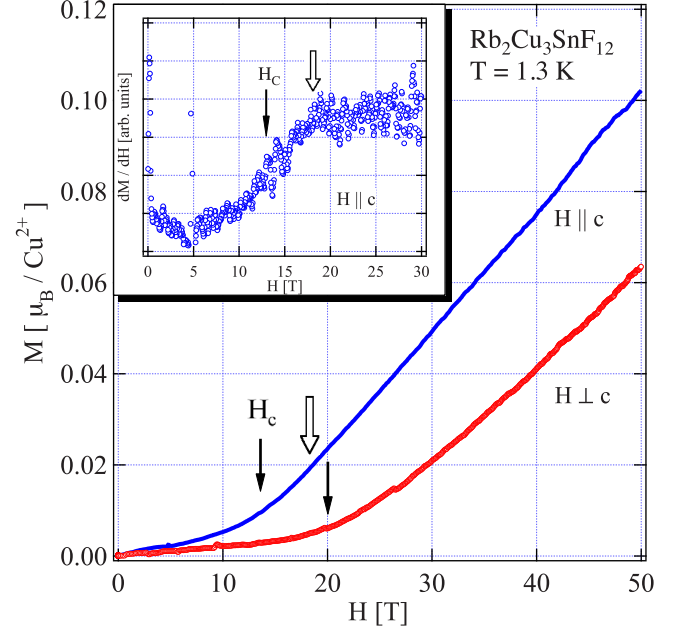


FIG. 8. (Color online) Magnetization curves of $\text{Rb}_2\text{Cu}_3\text{SnF}_{12}$ measured at $T=1.3$ K for $H \parallel c$ and $H \perp c$. Arrows indicate the critical field H_c . Inset shows dM/dH vs H for $H \parallel c$.

$=2.15(1)$. The average of the exchange constants is $J_{av} = 185$ K. Solid lines in Fig. 3(d) denote the susceptibilities calculated with these parameters. The magnitudes of these exchange interactions are valid from the fact that $J/k_B = 240$ K and $\alpha = 140.1^\circ$ in $\text{Cs}_2\text{Cu}_3\text{SnF}_{12}$ and $J/k_B = 103$ K and $\alpha = 129.1^\circ$ in KCuGaF_6 .⁷⁸ In these two antiferromagnets, the exchange interactions were determined with high accuracy. For $T < T_{\text{max}}$, the calculated susceptibility decreases more rapidly than the experimental susceptibility because of the finite-size effect. Calculation for a larger kagome cluster may give a better description of low-temperature susceptibility.

The exponential temperature variation of the low-temperature susceptibility indicates the presence of the triplet gap. The asymptotic low-temperature susceptibility for a two-dimensional (2D) gapped system with a parabolic dispersion above the gap Δ is expressed as^{79,80}

$$\chi = A \exp(-\Delta/k_B T). \quad (3)$$

The magnitude of the gap in $\text{Rb}_2\text{Cu}_3\text{SnF}_{12}$ is estimated to be $\Delta/k_B = 21(1)$ K by fitting Eq. (3) to the low-temperature susceptibility data for $H \parallel c$. The solid line in the inset of Fig. 3(d) denotes the fit.

We also performed high-field magnetization measurements to evaluate the triplet gap directly. Figure 8 shows magnetization curves and dM/dH vs H measured at $T = 1.3$ K for $H \parallel c$ and $H \perp c$. The magnetization is small up to the critical field H_c indicated by solid arrows and increases rapidly. This magnetization behavior is typical of the gapped spin system. Level crossing between the ground and excited states occurs at H_c . The bend anomaly at H_c is not sharp but is rather rounded. We infer that the smearing of the transition at H_c is ascribed to the staggered Zeeman and DM interac-

tions that are antisymmetric with respect to the interchange of spins. We assign the critical field H_c to the field of inflection in dM/dH as shown in the inset of Fig. 8. The critical fields obtained for $H\parallel c$ and $H\perp c$ are $H_c=13(1)$ and $20(1)$ T, respectively. These critical fields do not coincide when normalized with the g factor as $(g/2)H_c$. Because the magnetic susceptibility for $H\perp c$ is finite even at $T=0$, the ground state has a finite triplet component. Thus, the ground-state energy is no longer independent of the external field but decreases with the external field. This leads to an increase in the critical field. Therefore, we evaluate the gap to be $\Delta/k_B=21(1)$ K from $H_c=13(1)$ T obtained for $H\parallel c$. The magnitudes of the gap evaluated from the critical field and the low-temperature susceptibility coincide. However, there is a certain amount of error in determining the critical field H_c because the bend anomaly at H_c is smeared. If we assign H_c to the field indicated by outlined arrow at which dM/dH becomes constant with increasing external field, we obtain $H_c=18(1)$ T for $H\parallel c$, which leads to $\Delta/k_B=30(1)$ K. Anyway, the magnitude of the triplet gap is of the order of $1/10$ of J_{av} .

It is evident from the present measurements that the ground state of $\text{Rb}_2\text{Cu}_3\text{SnF}_{12}$ is a spin singlet with a triplet gap, while $\text{Cs}_2\text{Cu}_3\text{SnF}_{12}$ has an ordered ground state. Then, we discuss the cause of the different ground states in these systems. Although the crystal lattice of $\text{Cs}_2\text{Cu}_3\text{SnF}_{12}$ is enlarged to $2a\times 2a$ below the structural phase transition at $T_t=185$ K, the deviation of the magnetic susceptibility from the theoretical susceptibility for the uniform HKAF is small down to 30 K. This implies that the dispersion of the exchange constant ($J_1\sim J_4$) in $\text{Cs}_2\text{Cu}_3\text{SnF}_{12}$ is smaller than that in $\text{Rb}_2\text{Cu}_3\text{SnF}_{12}$. The triplet gap produced in a kagome layer decreases with decreasing dispersion of the exchange constant. Conversely, the gap increases with increasing degree of dimerization. Therefore, the gap produced in a kagome layer should be smaller in $\text{Cs}_2\text{Cu}_3\text{SnF}_{12}$ than in $\text{Rb}_2\text{Cu}_3\text{SnF}_{12}$ and the gap in $\text{Cs}_2\text{Cu}_3\text{SnF}_{12}$ collapses more easily when weak interlayer interaction operates. Because the distances between kagome layers in $\text{Cs}_2\text{Cu}_3\text{SnF}_{12}$ and $\text{Rb}_2\text{Cu}_3\text{SnF}_{12}$ are almost the same, the interlayer exchange interactions in both systems are of the same order of magnitude. We infer that the difference between the gaps produced by the exchange interactions in the kagome layers of both systems is an important factor of the different ground states.

We consider the difference in magnitude of the parallel component of the \mathbf{D} vector as the second factor leading to the different ground state between $\text{Cs}_2\text{Cu}_3\text{SnF}_{12}$ and $\text{Rb}_2\text{Cu}_3\text{SnF}_{12}$. Recently, Cépas *et al.*⁸¹ discussed the effect of the DM interaction on the ground state of $S=1/2$ HKAF. The configuration of the \mathbf{D} vectors that they assumed is the same as that shown in Fig. 4. Using exact diagonalization and finite-size scaling, they argued that with increasing parallel component D^{\parallel} , a quantum phase transition from a gapped state to an ordered state occurs and that the quantum critical point is given by $D_c^{\parallel}\approx 0.1J$. In the present systems, the magnitude of the \mathbf{D} vector is roughly estimated to be $D\sim(\Delta g/J)J=0.2J$,⁷⁰ with $\Delta g\approx 0.45$. Because ESR spectrum

was not observed because of the extremely large linewidth produced by the large DM interaction,⁶⁸ the ratio of D^{\parallel} to D^{\perp} is unclear. However, it is probable that D^{\parallel} exceeds $0.1J$ so that the ground state is gapless for triplet excitations. In this case, 3D ordering occurs at finite temperature with the help of interlayer interactions, as observed in $\text{Cs}_2\text{Cu}_3\text{SnF}_{12}$.

IV. CONCLUSIONS

We have presented the results of magnetic-susceptibility measurements on the single crystals of $\text{Cs}_2\text{Cu}_3\text{MF}_{12}$ ($M=\text{Zr, Hf, and Sn}$), which are described as $S=1/2$ HKAF. In these systems, structural phase transitions were observed at $T_t=225, 172,$ and 185 K for $M=\text{Zr, Hf, and Sn}$, respectively. The magnetic susceptibilities observed for $T>T_t$ are almost perfectly described using theoretical susceptibilities obtained by exact diagonalization for the 24-site kagome cluster with the exchange parameters and the g factors shown in Table III. For $\text{Cs}_2\text{Cu}_3\text{SnF}_{12}$, the agreement between theoretical and experimental susceptibilities is fairly good even below T_t . The magnetic susceptibility exhibits a rounded maximum at $T_{\max}\approx 38$ K, which coincides with the theoretical result $T_{\max}\approx(1/6)J/k_B$. Magnetic ordering accompanied by the weak ferromagnetic moment occurs at $T_N=23.5, 24.5,$ and 20.0 K for $M=\text{Zr, Hf, and Sn}$, respectively. The origins of the weak ferromagnetic moments parallel and perpendicular to the kagome layer should be ascribed to the lattice distortion that breaks the hexagonal symmetry of the exchange network for $T<T_t$ and the perpendicular component of the \mathbf{D} vector (D^{\perp}) for the DM interaction, respectively.

We have also presented the results of magnetic measurements on $\text{Rb}_2\text{Cu}_3\text{SnF}_{12}$, which is described as a modified kagome antiferromagnet with four types of exchange interactions. The results of magnetic susceptibility and high-field magnetization measurements revealed that the ground state is a spin singlet with a triplet gap. Using exact diagonalization for a 12-site kagome cluster, we analyzed the magnetic susceptibility and evaluated individual exchange interactions. We have discussed the causes leading to the different ground states in $\text{Cs}_2\text{Cu}_3\text{SnF}_{12}$ and $\text{Rb}_2\text{Cu}_3\text{SnF}_{12}$. We infer that the difference in the dispersion of the exchange constant in the kagome layer and/or in the magnitude of the parallel component of the \mathbf{D} vector causes the different ground states in these two systems.

ACKNOWLEDGMENTS

We express our sincere thanks to G. Misguich for showing us his theoretical calculations of magnetic susceptibility. This work was supported by a Grant-in-Aid for Scientific Research (A) from the Japan Society for the Promotion of Science and by a Global COE Program ‘‘Nanoscience and Quantum Physics’’ at Tokyo Tech and a Grant-in-Aid for Scientific Research on Priority Areas ‘‘High Field Spin Science in 100 T’’ which are both funded by the Japanese Ministry of Education, Culture, Sports, Science and Technology.

*o-toshio@lee.phys.titech.ac.jp

- ¹A. Harrison, J. Phys.: Condens. Matter **16**, S553 (2004).
- ²G. Misguich and C. Lhuillier, in *Frustrated Spin Systems*, edited by H. T. Diep (World Science, Singapore, 2005), p. 229.
- ³A. B. Harris, C. Kallin, and A. J. Berlinsky, Phys. Rev. B **45**, 2899 (1992).
- ⁴A. Chubukov, Phys. Rev. Lett. **69**, 832 (1992).
- ⁵J. N. Reimers and A. J. Berlinsky, Phys. Rev. B **48**, 9539 (1993).
- ⁶C. Zeng and V. Elser, Phys. Rev. B **42**, 8436 (1990).
- ⁷S. Sachdev, Phys. Rev. B **45**, 12377 (1992).
- ⁸J. T. Chalker and J. F. G. Eastmond, Phys. Rev. B **46**, 14201 (1992).
- ⁹N. Elstner and A. P. Young, Phys. Rev. B **50**, 6871 (1994).
- ¹⁰T. Nakamura and S. Miyashita, Phys. Rev. B **52**, 9174 (1995).
- ¹¹C. Zeng and V. Elser, Phys. Rev. B **51**, 8318 (1995).
- ¹²K. Hida, J. Phys. Soc. Jpn. **69**, 4003 (2000).
- ¹³K. Hida, J. Phys. Soc. Jpn. **70**, 3673 (2001).
- ¹⁴P. Lecheminant, B. Bernu, C. Lhuillier, L. Pierre, and P. Sindzingre, Phys. Rev. B **56**, 2521 (1997).
- ¹⁵Ch. Waldtmann, H.-U. Everts, B. Bernu, C. Lhuillier, P. Sindzingre, P. Lechminant, and L. Pierre, Eur. Phys. J. B **2**, 501 (1998).
- ¹⁶F. Mila, Phys. Rev. Lett. **81**, 2356 (1998).
- ¹⁷A. V. Syromyatnikov and S. V. Maleyev, Phys. Rev. B **66**, 132408 (2002).
- ¹⁸H. C. Jiang, Z. Y. Weng, and D. N. Sheng, Phys. Rev. Lett. **101**, 117203 (2008).
- ¹⁹P. Nikolic and T. Senthil, Phys. Rev. B **68**, 214415 (2003).
- ²⁰R. Budnik and A. Auerbach, Phys. Rev. Lett. **93**, 187205 (2004).
- ²¹R. R. P. Singh and D. A. Huse, Phys. Rev. B **76**, 180407(R) (2007).
- ²²R. R. P. Singh and D. A. Huse, Phys. Rev. B **77**, 144415 (2008).
- ²³B.-J. Yang, Y. B. Kim, J. Yu, and K. Park, Phys. Rev. B **77**, 224424 (2008).
- ²⁴M. Mambrini and F. Mila, Eur. Phys. J. B **17**, 651 (2000).
- ²⁵M. B. Hastings, Phys. Rev. B **63**, 014413 (2000).
- ²⁶S. Ryu, O. I. Motrunich, J. Alicea, and M. P. A. Fisher, Phys. Rev. B **75**, 184406 (2007).
- ²⁷Y. Ran, M. Hermele, P. A. Lee, and X.-G. Wen, Phys. Rev. Lett. **98**, 117205 (2007).
- ²⁸M. Hermele, Y. Ran, P. A. Lee, and X.-G. Wen, Phys. Rev. B **77**, 224413 (2008).
- ²⁹G. Misguich and P. Sindzingre, Eur. Phys. J. B **59**, 305 (2007).
- ³⁰M. Takano, T. Shinjo, M. Kiyama, and T. Takada, J. Phys. Soc. Jpn. **25**, 902 (1968).
- ³¹M. Takano, T. Shinjo, and T. Takada, J. Phys. Soc. Jpn. **30**, 1049 (1971).
- ³²M. G. Townsend, G. Longworth, and E. Roudaut, Phys. Rev. B **33**, 4919 (1986).
- ³³S. Maegawa, M. Nishiyama, N. Tanaka, A. Oyamada, and M. Takano, J. Phys. Soc. Jpn. **65**, 2776 (1996).
- ³⁴A. S. Wills, A. Harrison, C. Ritter, and R. I. Smith, Phys. Rev. B **61**, 6156 (2000).
- ³⁵T. Inami, M. Nishiyama, S. Maegawa, and Y. Oka, Phys. Rev. B **61**, 12181 (2000).
- ³⁶A. S. Wills, Phys. Rev. B **63**, 064430 (2001).
- ³⁷T. Inami, T. Morimoto, M. Nishiyama, S. Maegawa, Y. Oka, and H. Okumura, Phys. Rev. B **64**, 054421 (2001).
- ³⁸A. S. Wills, G. S. Oakley, D. Visser, J. Frunzke, A. Harrison, and K. H. Andersen, Phys. Rev. B **64**, 094436 (2001).
- ³⁹T. Morimoto, M. Nishiyama, S. Maegawa, and Y. Oka, J. Phys. Soc. Jpn. **72**, 2085 (2003).
- ⁴⁰D. Grohol, D. G. Nocera, and D. Papoutsakis, Phys. Rev. B **67**, 064401 (2003).
- ⁴¹M. Nishiyama, S. Maegawa, T. Inami, and Y. Oka, Phys. Rev. B **67**, 224435 (2003).
- ⁴²D. Grohol, K. Matan, J.-H. Cho, S.-H. Lee, J. W. Lynn, D. G. Nocera, and Y. S. Lee, Nature Mater. **4**, 323 (2005).
- ⁴³M. Leblanc, R. De Pape, G. Ferey, and J. Pannetier, Solid State Commun. **58**, 171 (1986).
- ⁴⁴M. Elhajal, B. Canals, and C. Lacroix, Phys. Rev. B **66**, 014422 (2002).
- ⁴⁵A. S. Wills, A. Harrison, S. A. M. Mentink, T. E. Mason, and Z. Tun, Europhys. Lett. **42**, 325 (1998).
- ⁴⁶B. Fåk, F. C. Coomer, A. Harrison, D. Visser, and M. E. Zhitomirsky, Europhys. Lett. **81**, 17006 (2008).
- ⁴⁷N. Wada, T. Kobayashi, H. Yano, T. Okuno, A. Yamaguchi, and K. Awaga, J. Phys. Soc. Jpn. **66**, 961 (1997).
- ⁴⁸T. Kambe, Y. Nogami, K. Oshima, W. Fujita, and K. Awaga, J. Phys. Soc. Jpn. **73**, 796 (2004).
- ⁴⁹Z. Hiroi, M. Hanawa, N. Kobayashi, M. Nohara, H. Takagi, Y. Kato, and M. Takigawa, J. Phys. Soc. Jpn. **70**, 3377 (2001).
- ⁵⁰Z. Honda, K. Katsumata, and K. Yamada, J. Phys.: Condens. Matter **14**, L625 (2002).
- ⁵¹N. Rogado, M. K. Haas, G. Lawes, D. A. Huse, A. P. Ramirez, and R. J. Cava, J. Phys.: Condens. Matter **15**, 907 (2003).
- ⁵²Y. Narumi, K. Katsumata, Z. Honda, J.-C. Domenge, P. Sindzingre, C. Lhuillier, Y. Shimaoka, T. C. Kobayashi, and K. Kindo, Europhys. Lett. **65**, 705 (2004).
- ⁵³M. P. Shores, E. A. Nytko, B. M. Bartlett, and D. G. Nocera, J. Am. Chem. Soc. **127**, 13462 (2005).
- ⁵⁴P. Mendels, F. Bert, M. A. de Vries, A. Olariu, A. Harrison, F. Duc, J. C. Trombe, J. S. Lord, A. Amato, and C. Baines, Phys. Rev. Lett. **98**, 077204 (2007).
- ⁵⁵J. S. Helton, K. Matan, M. P. Shores, E. A. Nytko, B. M. Bartlett, Y. Yoshida, Y. Takano, A. Suslov, Y. Qiu, J.-H. Chung, D. G. Nocera, and Y. S. Lee, Phys. Rev. Lett. **98**, 107204 (2007).
- ⁵⁶F. Bert, S. Nakamae, F. Ladieu, D. L'Hôte, P. Bonville, F. Duc, J.-C. Trombe, and P. Mendels, Phys. Rev. B **76**, 132411 (2007).
- ⁵⁷M. Rigol and R. R. P. Singh, Phys. Rev. Lett. **98**, 207204 (2007).
- ⁵⁸M. Rigol and R. R. P. Singh, Phys. Rev. B **76**, 184403 (2007).
- ⁵⁹S.-H. Lee, H. Kikuchi, Y. Qiu, B. Lake, Q. Huang, K. Habicht, and K. Kiefer, Nature Mater. **6**, 853 (2007).
- ⁶⁰T. Imai, E. A. Nytko, B. M. Bartlett, M. P. Shores, and D. G. Nocera, Phys. Rev. Lett. **100**, 077203 (2008).
- ⁶¹A. Olariu, P. Mendels, F. Bert, F. Duc, J. C. Trombe, M. A. de Vries, and A. Harrison, Phys. Rev. Lett. **100**, 087202 (2008).
- ⁶²M. A. de Vries, K. V. Kamenev, W. A. Kockelmann, J. Sanchez-Benitez, and A. Harrison, Phys. Rev. Lett. **100**, 157205 (2008).
- ⁶³A. Zorko, S. Nellutla, J. van Tol, L. C. Brunel, F. Bert, F. Duc, J.-C. Trombe, M. A. de Vries, A. Harrison, and P. Mendels, Phys. Rev. Lett. **101**, 026405 (2008).
- ⁶⁴M. Müller and B. G. Müller, Z. Anorg. Allg. Chem. **621**, 993 (1995).
- ⁶⁵Y. Yamabe, T. Ono, T. Suto, and H. Tanaka, J. Phys.: Condens. Matter **19**, 145253 (2007).
- ⁶⁶K. Morita, M. Yano, T. Ono, H. Tanaka, K. Fujii, H. Uekusa, Y. Narumi, and K. Kindo, J. Phys. Soc. Jpn. **77**, 043707 (2008).
- ⁶⁷P. W. Selwood, *Magnetochemistry*, 2nd ed. (Interscience, New York, 1956), Chap. 2, p. 78.

- ⁶⁸The origin of the ESR linewidth ΔH is considered to be the DM interaction. The linewidth is given by $\Delta H \sim D^2 / (g\mu_B J)$. The magnitude of the D vector is roughly given by $D \sim (\Delta g / g) J$ (Ref. 70). Using $\Delta g \approx 0.45$ and $J/k_B \approx 250$ K, we estimate the linewidth to be $\Delta H \sim 10$ T. This linewidth is too large to be observed by conventional ESR technique.
- ⁶⁹S. Sasaki, N. Narita, and I. Yamada, J. Phys. Soc. Jpn. **64**, 2701 (1995).
- ⁷⁰T. Moriya, Phys. Rev. **120**, 91 (1960).
- ⁷¹H. Tanaka, F. Tsuruoka, T. Ishii, H. Izumi, K. Iio, and K. Nagata, J. Phys. Soc. Jpn. **55**, 2369 (1986).
- ⁷²F. Wang, A. Vishwanath, and Y. B. Kim, Phys. Rev. B **76**, 094421 (2007).
- ⁷³T. Yavors'kii, W. Apel, and H.-U. Everts, Phys. Rev. B **76**, 064430 (2007).
- ⁷⁴T. Kato, K. Iio, T. Hoshino, T. Mitsui, and H. Tanaka, J. Phys. Soc. Jpn. **61**, 275 (1992).
- ⁷⁵I. Affleck and M. Oshikawa, Phys. Rev. B **60**, 1038 (1999).
- ⁷⁶D. A. Tennant, T. G. Perring, R. A. Cowley, and S. E. Nagler, Phys. Rev. Lett. **70**, 4003 (1993).
- ⁷⁷H. Manaka, Y. Miyashita, Y. Watanabe, and T. Masuda, J. Phys. Soc. Jpn. **76**, 044710 (2007).
- ⁷⁸R. Morisaki, T. Ono, H. Tanaka, and H. Nojiri, J. Phys. Soc. Jpn. **76**, 063706 (2007).
- ⁷⁹M. Troyer, H. Tsunetsugu, and D. Würtz, Phys. Rev. B **50**, 13515 (1994).
- ⁸⁰M. B. Stone, I. Zaliznyak, D. H. Reich, and C. Broholm, Phys. Rev. B **64**, 144405 (2001).
- ⁸¹O. Cépas, C. M. Fong, P. W. Leung, and C. Lhuillier, Phys. Rev. B **78**, 140405(R) (2008).